

# Andreev and Majorana bound states in single and double quantum dot structures

**Joelson F. Silva and E. Vernek**

Instituto de Física, Universidade Federal de Uberlândia, Uberlândia, Minas Gerais  
38400-902, Brazil.

E-mail: vernek@ufu.br

**Abstract.** We present a numerical study of the emergence of Majorana and Andreev bound states in a system composed by two quantum dots, in which one of them is coupled to a conventional superconductor, SC1, and the other connects to a topological superconductor, SC2. By controlling the interdot coupling we can drive the system from a two single (uncoupled) quantum dots to a double (coupled) dot system configurations. We employ a recursive Green's function technique that provides us with numerically exact results for the local density of states of the system. We first show that in the uncoupled dot configuration (single dot behavior) the Majorana and the Andreev bound states appear in an individual dot in two completely distinct regimes. Therefore, they cannot coexist in the single quantum dot system. We then study the coexistence of these states in the coupled double-dot configuration. In this situation we show that in the trivial phase of the SC2, the Andreev states are bound to an individual quantum dot in the atomic regime (weak interdot coupling) or extended over the entire molecule in the molecular regime (strong interdot coupling). More interesting features are actually seen in the topological phase of the SC2. In this case, in the atomic limit, the Andreev states appear bound to one of the quantum dots while a Majorana zero mode appears in the other one. In the molecular regime, on the other hand, the Andreev bound states take over the entire molecule while the Majorana state remains always bound to one of the quantum dots.

PACS numbers: 03.67.Lx, 71.10.Pm, 73.63.Kv, 74.25.F-, 74.45.+c, 73.21.La

*Keywords:* Topological superconductors, Andreev bound states, Majorana fermions.

## 1. Introduction

Nanoscale structures coupled to superconductors has attracted the attention of many researchers over the last two decades [1–9]. One interesting aspect of nanostructured systems such as quantum dots coupled to normal or superconducting contacts is their flexibility to study many different phenomena, such as the Kondo effect [10], the Andreev bound states (ABS), etc. Due to confinement, quantum dot systems exhibit a discrete spectrum that can be modified by local gates, allowing for a fine control of their physical properties.

When a quantum dot is connected to a conventional superconductor, multiple Andreev reflections between the quantum dot and the superconductor give rise to Andreev bound states (ABS) in the dot [11, 12], with signature visible in their transport properties [13, 14]. For example, by studying a graphene quantum dot coupled to a normal and to a superconductor contacts, Dirks et al [13] have observed sharp *in gap* conductance peaks attributed to individual ABS in the system. Another interesting result is the interplay between the Kondo screening and the superconducting pairing in quantum dots observed by Pillet et al [6]. Interplay between Kondo and Andreev bound states has also been studied earlier by Franke and coworkers [9], in magnetic molecules on the surface of a superconductor.

More recently, quantum dots coupled to topological superconductor wires [15–18] supporting Majorana bound states (MBS) in their ends have also attracted a lot of attention. Besides the interest in the fundamental concepts of the Majorana state physics [19–21], it is also potentially useful for topologically protected quantum computation [22–27]. Despite the great effort of various researchers toward experimental observation [28–30], no much progress have been made lately. One of the most challenging task

for a clear observation of MBS features in condensed matter systems is to tell apart features from other phenomena, as it has been argued that MBS may be confused with signatures from Kondo or ABS. For instance, it has been shown by one of us that, under certain regime, the Majorana and the Kondo physics can coexist in a quantum dot that is simultaneously coupled to a topological superconductor and to a metallic contact [17, 32]. Therefore, identifying features of a particular phenomena can be experimentally puzzling. While the interplay between the Majorana and the Kondo effect have been investigated in some detail, very little attention have been devoted to MBS and ABS together [33, 34]. For instance, do MBS and ABS mix together? More importantly, if the MBS and ABS coexist in some regime, how can one distinguish them experimentally? The answer to these important questions still remain unclear.

Aiming to addressing these questions, in this work we investigate possible coexistence and interplay between Andreev and Majorana bound states in a single and double dot systems. We consider a double quantum dot system in which

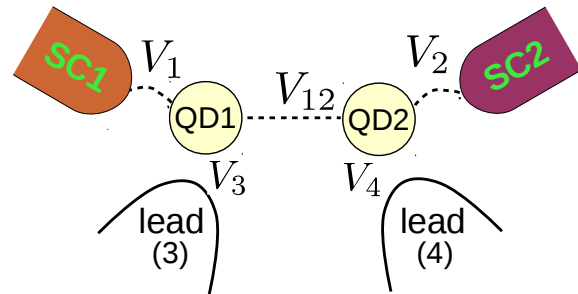


**Figure 1.** (Color online) Schematic representation of the system. SC1 and SC2 represent a conventional *s*-wave and a topological superconductor, respectively. The terminals 3 and 4 are normal metallic leads that introduces a natural broadening of each quantum dot spectrum. QD1 and QD2 represents single level and non-interacting quantum dots. By controlling  $V_{12}$  we can drive the system from a two single (uncoupled) dots to a double (coupled) dot configurations.

one of the dots is coupled to a conventional superconductor while the other couples to topological superconductor. The quantum dots are interconnected by a controllable tunneling barrier that allows us to drive the system from a single to a double dot configurations, providing a flexible structure to address possible mixing of MBS and ABS. For the sake of clarity, our system, schematically represented in Fig. 1. It resembles the one proposed by Pillet et al, in Ref. [6]. Here, however, while the left quantum dot (QD1) is coupled to a normal  $s$ -wave superconductor (SC1) the right one (QD2) is connected to a topological superconductor that provides the Majorana bound state. Furthermore, each of the QDs are coupled to individual metallic leads labeled by (3) and (4) (see Fig. 1) that induces a natural broadening of the QD levels. When the QDs are decoupled from each other, if the SC2 is in its topological phase, a Majorana mode will appear in the QD2, as predicted in Ref. [32], while in the QD1 there will be a pair of ABSs.

To study the bound states we focus mainly on the spectral properties of the system, that is accessible via zero-bias differential conductance measurement as in experiment reported in Ref. [6]. We employ the standard recursive Green's function approach, from which we can obtain numerically exact results for the local density of states of the system. We first study the situation in which the QDs are fully decoupled from each other. In this configuration we monitor the local density of states of the QD2 while driving the SC2 from its trivial to its topological phase. We show that the MBS and the ABSs appear in two distinct regimes, that can be distinguished in tunneling spectroscopy measurements. We then go on and study possible coexistence of MBS and ABS in the double dot configuration. To do so we couple the two QDs by making the interdot coupling finite. We find that in the trivial phase of the SC2 and in the atomic limit (small interdot

coupling) the dot coupled to the normal superconductor exhibits the usual Andreev bound states whereas the other one exhibits a atomic single particle peak. In the molecular regime (strong interdot coupling), the Andreev states take over the entire molecule, appearing clearly in the molecular orbitals. More interestingly, in the topological phase of the SC2, in the atomic regime we see Andreev bound states in the QD1 and a Majorana zero mode in the QD2. In the molecular regime, on the other hand, while the Andreev bound states is seen over entire molecule, the Majorana mode (seen only for spin *down*) is always bound to an atomic orbital.

The remainder of this paper is structured in the following way. In Sec. 2 we describe the model and derive the main physical quantities and in Sec. 3 we present our numerical results. Finally, we conclude our work in Sec. 4.

## 2. Model and method

### 2.1. Hamiltonian model

For concreteness, our system is described by the following Hamiltonian:

$$H = H_{\text{dots}} + H_{\text{SC}} + H_{\text{leads}} + H_{\text{dot-leads}} + H_{\text{dot-SC}} + H_{\text{T}}. \quad (1)$$

Here  $H_{\text{dots}}$  and  $H_{\text{leads}}$  describes the isolated quantum dots and the normal leads, respectively,  $H_{\text{SC}} = H_1 + H_2$  describes the normal and the topological superconductors,  $H_{\text{dot-leads}}$  connects the dot to the normal leads,  $H_{\text{dot-SC}}$  couples the dots the superconductors and  $H_{\text{T}}$  describes the tunnel coupling between the dots. Explicitly, the various terms in the Hamiltonian (1) can be written as,

$$H_{\text{dots}} = \sum_{i=1,2} \sum_s \epsilon_{i,s} d_{i,s}^\dagger d_{i,s}, \quad (2)$$

$$H_1 = \sum_{j=-\infty}^{-1} \sum_s \left( t_1 c_{j-1,s}^\dagger c_{j,s} + \Delta_1 c_{j,\uparrow}^\dagger c_{j,\downarrow}^\dagger + \text{H.c.} \right), \quad (3)$$

$$H_2 = \frac{1}{2} \sum_{j=1,s}^{\infty} \left[ (-\mu + V_Z \sigma_{ss}^z) c_{j,s}^{\dagger} c_{j,s} - t_2 c_{j+1,s}^{\dagger} c_{j,s} + \Delta_2 c_{j,\uparrow}^{\dagger} c_{j,\downarrow}^{\dagger} \right] + it_{SO} \sum_{j=1,ss'}^{\infty} (c_{j+1,s}^{\dagger} \sigma_{ss'}^y c_{j,s'}) + \text{H.c.}, \quad (4)$$

$$H_{\text{leads}} = \sum_{\ell, \mathbf{k}, s} \varepsilon_{\ell, \mathbf{k}, s} c_{\ell, \mathbf{k}, s}^{\dagger} c_{\ell, \mathbf{k}, s} \quad (\ell = 3, 4), \quad (5)$$

$$H_{\text{dot-leads}} = \sum_{\mathbf{k}, s} (V_3 d_{1,s}^{\dagger} c_{3, \mathbf{k}, s} + V_4 d_{2,s}^{\dagger} c_{4, \mathbf{k}, s} + \text{H.c.}), \quad (6)$$

$$H_{\text{dot-SC}} = - \sum_s (V_1 d_{1,s}^{\dagger} c_{-1,s} + V_2 d_{2,s}^{\dagger} c_{1,s}) + \text{H.c.}, \quad (7)$$

and

$$H_T = -V_{12} \sum_s (d_{1,s}^{\dagger} d_{2,s} + d_{2,s}^{\dagger} d_{1,s}). \quad (8)$$

In the Eqs. (2)-(8),  $d_{i,s}^{\dagger}$  ( $d_{i,s}$ ) creates (annihilates) an electron with energy  $\varepsilon_{i,s}$  and spin  $s$  in the quantum dot  $i = 1, 2$ ,  $c_{j,s}^{\dagger}$  ( $c_{j,s}$ ) creates (annihilates) an electron with spin  $s$  in the  $j$ -th site of the superconductors and  $c_{\ell, \mathbf{k}}^{\dagger}$  ( $c_{\ell, \mathbf{k}}$ ) creates (annihilates) an electron with energy  $\varepsilon_{\ell, \mathbf{k}}$  with spin  $s$  in the  $\ell$ -th lead. Note that, besides the  $s$ -wave pairing potential  $\Delta_2$  of  $H_2$ , it also contains a Rashba spin-orbit interaction characterized by the  $t_{SO}$  and the effect of an external magnetic field that produces the Zeeman energy splitting  $V_z$ . These three ingredients are important for the topological regime of the superconductor [28, 31]. The coupling  $V_{3(4)}$  are assumed to be  $\mathbf{k}$ -independent, for simplicity, and the leads are considered to be identical and characterized by a flat density of states  $\rho_0(\omega) = (1/2D)\Theta(D - |\omega|)$ , where  $D$  is their half bandwidth. In the wide band limit, the influence of the lead on the dots are just a broadening  $\Gamma = \pi V^2/2D$  in the QD levels, where  $V_3 = V_4 = V$ . The wide band limit for the leads assumed here just simplifies the equations but it is not mandatory. In this limit, our calculation fully accounts the effect of the leads.

The topological phase of the SC2, described by the Hamiltonian (4), is obtained [35] for  $V_Z > V_Z^c$ , where  $V_Z^c = \sqrt{\tilde{\mu}^2 + \Delta_2^2}$ , with  $\tilde{\mu} = \mu + t$ . In this phase, the SC2 holds one Majorana mode at each of its ends. In our case, one of the ends of the topological wire is coupled to QD2 and the Majorana mode leaks into it, as we have shown in recent studies [32, 36]. On the other hand, for  $V_Z < V_Z^c$  the wire is in its trivial phase and no Majorana will be present.

## 2.2. Electron Green's function

To study the local density of states (LDOS) of the QDs we employ the Green's function (GF) method. Using the equation of motion techniques we obtain a recursive expression for the GFs. We follow a similar approach as described in Ref. [36] and define the retarded GF matrix as

$$\mathbf{G}_{i,j}(\varepsilon) \equiv \langle\langle A_i; B_j \rangle\rangle, \quad (9)$$

where  $A_i$  and  $B_i$  (with  $i$  and  $j$  denoting any site of the system (including the quantum dots) are any of the operators  $c_{i\uparrow}, c_{i\downarrow}, c_{i\uparrow}^{\dagger}, c_{i\downarrow}^{\dagger}$  and the double bracket stands for the Fourier transform of the double time GF defined as [37]

$$\langle\langle A_i; B_j \rangle\rangle = \int_{-\infty}^{\infty} (-i)\Theta(\tau) \langle [A_i(t), B_j(t')]_+ \rangle e^{i\varepsilon\tau} d\tau. \quad (10)$$

Here  $\tau = t - t'$  and  $[\cdot, \cdot]_+$  denotes the anticommutator between two fermion operators. The GF (9) defines a  $4 \times 4$  matrix that is determined via energy space equation of motion for its elements

$$\varepsilon \langle\langle A_i; B_j \rangle\rangle = \langle [A_i; B_j]_+ \rangle + \langle\langle [A_i; H], B_j \rangle\rangle. \quad (11)$$

Since there are no many-body terms in the Hamiltonian, the Eq. (11) allow us to obtain numerically exact results including all the contacts (see details in Ref. [36]). Once we have the local GFs, we can compute the local density of states of the QDs sites,

$$\rho_i^s(\varepsilon) = -\frac{1}{\pi} \text{Im} [\langle\langle d_{i,s}; d_{i,s}^{\dagger} \rangle\rangle], \quad (12)$$

that can be readily extracted from the matrix GF (9).

As far as the interdot coupling concerns, it is well known that our double QD system exhibits two distinct regimes: the atomic regime, for  $V_{12} \ll \Gamma$ , and the molecular regime, for  $V_{12} \gg \Gamma$ . In the atomic regime, because the electrons are more bound to the individual QD orbitals, the spectral properties of the system is better understood in terms of local density of states given by the Eq. (12). On the other hand, in the molecular regime (in which electrons are shared between the QDs) the spectral properties can be better understood in terms of molecular density of states. To analyze the later regime we define two molecular orbitals,

$$d_{\pm,s} = \frac{1}{\sqrt{2}}(d_{1,s} \pm d_{2,s}) \quad (13)$$

that provide us with the molecular density of states

$$\rho_{\pm}^s(\varepsilon) = -\frac{1}{\pi} \text{Im} [\langle\langle d_{\pm,s}; d_{\pm,s}^\dagger \rangle\rangle]. \quad (14)$$

This expression can be written in terms of the local and non-local quantum dot GFs as

$$\rho_{\pm}^s(\varepsilon) = \frac{\rho_1^s + \rho_2^s}{2} \mp \frac{1}{2\pi} \text{Im} [\langle\langle d_{1,s}; d_{2,s}^\dagger \rangle\rangle + \langle\langle d_{2,s}; d_{1,s}^\dagger \rangle\rangle], \quad (15)$$

where the non-local GFs,  $\langle\langle d_{1,s}; d_{2,s}^\dagger \rangle\rangle$  and  $\langle\langle d_{2,s}; d_{1,s}^\dagger \rangle\rangle$  appearing on the rhs of this expression are easily obtained by our procedure. Note that the interdot GF vanishes as  $V_{12} \rightarrow 0$ . Therefore, in this case, the molecular density of states is just the average of the QD (“atomic”) density of states.

### 2.3. Majorana Green's function

From the theoretical point of view, it is useful to define the Majorana GF

$$M_{\alpha i, \alpha i}^s(\varepsilon) \equiv \langle\langle \gamma_{\alpha i}^s; \gamma_{\alpha i}^s \rangle\rangle \quad (\text{for } \alpha = A, B), \quad (16)$$

where

$$\gamma_{Ai}^s = \frac{1}{2}(f_{i,s} + f_{i,s}^\dagger) \quad (17)$$

$$\gamma_{Bi}^s = -\frac{i}{2}(f_{i,s} - f_{i,s}^\dagger) \quad (18)$$

are the Majorana operators with the property

$$\gamma_{\alpha i}^s = (\gamma_{\alpha i}^s)^\dagger \quad (19)$$

and obeying the anti-commutation relation

$$[\gamma_{\alpha i}^s, \gamma_{\alpha' j}^{s'}]_+ = 2\delta_{i,j}\delta_{\alpha\alpha'}\delta_{ss'}. \quad (20)$$

Once we have obtained the electron GF, the definitions of the Majorana operators (17) and (18) allows us to write the retarded Majorana GF in terms of the regular and the retarded Gorkov's GF as

$$M_{Ai, Ai}^s(\varepsilon) = \frac{1}{4} [\langle\langle f_{i,s}; f_{i,s}^\dagger \rangle\rangle + \langle\langle f_{i,s}^\dagger; f_{i,s} \rangle\rangle + \langle\langle f_{i,s}; f_{i,s} \rangle\rangle + \langle\langle f_{i,s}^\dagger; f_{i,s}^\dagger \rangle\rangle], \quad (21)$$

and

$$M_{Bi, Bi}^s(\varepsilon) = \frac{1}{4} [\langle\langle f_{i,s}; f_{i,s}^\dagger \rangle\rangle + \langle\langle f_{i,s}^\dagger; f_{i,s} \rangle\rangle - \langle\langle f_{i,s}; f_{i,s} \rangle\rangle - \langle\langle f_{i,s}^\dagger; f_{i,s}^\dagger \rangle\rangle]. \quad (22)$$

We can now compute the Majorana local spectral function (MLSF) as

$$\mathcal{D}_{\alpha i}^s(\varepsilon) = -\frac{1}{\pi} \text{Im}[M_{\alpha i, \alpha i}^s]. \quad (23)$$

Here,  $f_{i,s}$  represents any regular fermion in the system. In particular, for the quantum dots,  $f_{i,s}$  stands for  $d_{i,s}$ . Although the MLSF cannot be directly accessed in experiments, it will help us to tell whether the electron density of states are composed by two Majorana modes or by a single one.

### 3. Numerical results

To obtain our numerical results we will set the hopping  $t_1 = t_2 = t = 10$  meV and  $\Gamma = 5.0 \times 10^{-5}t$ . We also set  $\varepsilon_1 = \varepsilon_2 = 0$ . Following previous studies with realistic parameters [28, 38], we set  $\Delta_1 = \Delta_2 = 0.025t$ ,  $t_{\text{SO}} = 0.07t$ .

### 3.1. Single dot configuration

We first want to show that in the case of a single QD coupled to a superconductor, the regime in which there is a MBS in the system, the ABS are suppressed. To this end, let us consider in our system the situation in which the two QDs are decoupled from each other, by setting  $V_{12} = 0$ . Here we will show the suppression of the ABS in the QD2 as the SC2 is driven from its trivial to its topological phase. We do it by setting  $V_z = 0.05t$  and varying  $\mu$ . The results are shown in Fig. 2(a) and 2(b), where we show the color map of density of states at the QD2 vs  $\varepsilon$  and  $\mu$ . Here, in particular, we set  $V_2 = 0.008t$  so that the Andreev levels becomes very separated and, therefore, more visible. For  $\mu = 0$  we clearly see the ABS symmetrically placed about  $\varepsilon = 0$  for both spin species. The small splitting in the ABS is due to the Zeeman effect. Now, observe that as  $\mu$  decreases from 0 to  $-t$  the upper branch of the ABS is progressively suppressed (also for both spins). This is because the strong electron-hole asymmetry induced by the change of the chemical potential suppresses the probability of creating a hole in the SC2. Interestingly, we note that, after the upper branch of the ABS has faded out, within a small range of  $\mu$  (of the order of  $V_z$ ), we see the appearance of a peak at  $\varepsilon = 0$  for spin down only [Fig. 2(b)] (note that this feature is not seen for spin up). This region is precisely the topological phase of the SC2, in which the MBS leaks out from the SC2 into the QD2 (see discussion below). For further decrease of  $\mu$ , the SC2 returns to its trivial phase, in which there is no MBS nor ABS. The peaks of Figs. 2(a) and 2(b) would be interchanged if we had chosen the opposite sign of  $V_z$ .

The small range of  $\mu$  for which the SC2 is found in its topological phase can be readily understood from the topological condition  $V_z^2 \geq \tilde{\mu}^2 + \Delta^2$ , or  $\mu \in [-t - (V_z^2 - \Delta^2)^{1/2}, -t + (V_z^2 - \Delta^2)^{1/2}]$ .

For  $V_z = 0.05t$  and  $\Delta = 0.025t$  we expect the MBS to appear only for  $\mu$  approximately within the interval  $[-1.043t, -0.957t]$  (or, equivalently,  $-\mu/t$  within  $[0.957, 1.043]$ ) as seen in Fig. 2(b). Note that the zero mode is limited, precisely, within the two vertical dashed lines delimiting the calculated interval. The discontinuities are consistent with the topological phase transition already predicted in Ref. [19].

Now that we have shown the suppression of the ABS by the chemical potential, let us show how the “surviving” peak evolves with  $V_z$ , towards the MBS. In Figs. 2(c) and 2(d) (for spin up and down, respectively) we show the density of states for the QD2 vs  $\varepsilon$  and  $V_z$  for a fixed value of  $\mu = -1.01t$ , which is inside the region delimited by the two vertical lines in Fig. 2(b). Note that, essentially, nothing changes for the spin up density of states. When  $V_z$  surpasses

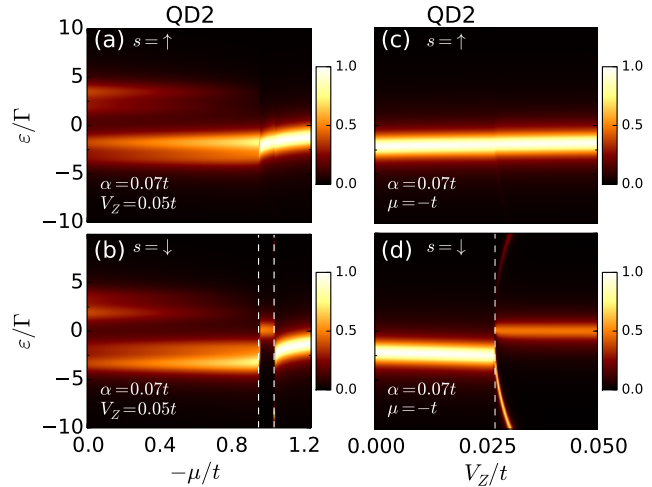


**Figure 2.** (Color online) Color map of the local density of states (in unity of  $1/\pi\Gamma$ ) of the QD2 as a function of the energy  $\varepsilon$  and  $\mu$  (left) and  $V_z$  (right). On the left, we have fixed  $V_z = 0.05t$  and vary  $\mu$  while on the right we fixed  $\mu = -1.01t$  and vary  $V_z$ . Top and bottom panels show the results for spin up and down, respectively. For all panels set  $V_{12} = 0$ , so there is no influence of the QD1, and  $V_1 = V_2 = 0.008t$ . The vertical dashed lines in the panels (b) and (c) delimit the boundary of the topological/trivial phase of the superconductor.

$V_Z^c$  there is a transition from the single to the tree-peak structure, in which the zero-energy peak corresponds to the MBS. The satellite peaks separate very quickly because the level of the QD2 is strongly coupled in resonance with the MBS from the wire. These peaks correspond to the Majorana state that is split off from the one that remains at energy zero. We will discuss this in the next subsection, when it will be more visible with a smaller values of  $V_Z$ . These results show that, indeed, ABS and the MBS cannot coexist in a single quantum dot.

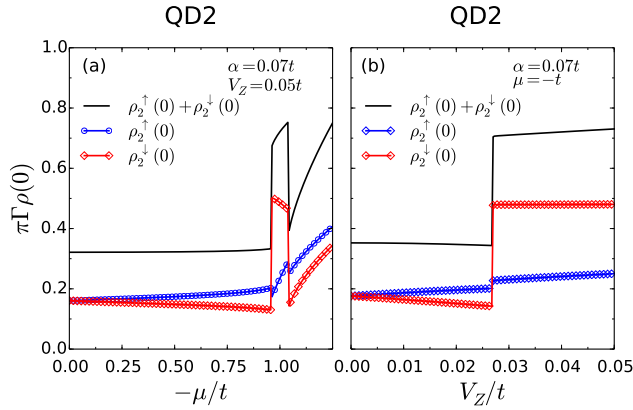


**Figure 3.** (Color online) Zero-energy LDOS vs chemical potential  $\mu$  (left) and Zeeman energy  $V_Z$  (right). The circles (blue) and the diamonds (red) curves correspond to the spin up and down, respectively, while the solid (black) lines corresponds to the total  $[\rho_2^\uparrow(0) + \rho_2^\downarrow(0)]$  density of states. These curves correspond to a cut along  $\varepsilon = 0$  in the panels of Fig. 2. All the other parameters are the same as those of Fig. 2.

As we have already mentioned above, experimentally, the signature of these features can be seen in the zero-bias differential conductance in spectroscopy tunneling measurements, that provide a probe of the LDOS at zero energy. To accomplish this, one can place an STM tip on top of the QD2 to measure the zero-bias conductance from the normal contact into the lead 2 into the tip. The observed conductance  $G \propto \rho_2(0) = \rho_2^\uparrow(0) + \rho_2^\downarrow(0)$  would be similar

to what is shown in Fig. 3 solid (black) curves. Setting the level of the QD2  $\varepsilon_2$  at the Fermi level of the lead 2 and  $V_Z$  finite, by varying  $\mu$  one would observe a very low conductance in the ABS regime. When the SC2 enters the topological phase, the conductance jumps to a very higher value, as seen in Fig. 3(a). Then after leaving the topological phase, the conductance would drop suddenly to a smaller value. For completeness, in Fig. 3(b) we show the same quantity as a function of  $V_Z$ . The topological phase transition in this case would again be seen in a discontinuity in the conductance. In this case, there is only one jump because the SC2 is in its topological phase for all  $V_Z > V_Z^c$ . This plot is quite different from that one found in the Figs. 2(c) and 2(d) of Ref. [16]. Note that, in contrast with the result of Ref. [16], here the conductance increases in the topological phase, while there the conductance decreases. This disagreement is because our approach accounts for the ABS fully, while in theirs there is no ABS.

### 3.2. Double dot configuration

Since the Majorana and the Andreev bound states live in the system in different regimes of the single dot structure, it is still interesting to investigate possible interplay between these bound states with MBS in the double QD configuration. Here, the SC1 is treated as a conventional superconductor (i.e., no spin-orbit, nor Zeeman field), whereas the SC2 is considered either in its normal phase ( $V_Z < V_Z^c$ ) and in its topological phase ( $V_Z > V_Z^c$ ), with  $V_Z^c = \sqrt{\tilde{\mu}^2 + \Delta^2}$ . Then we make the coupling  $V_{12}$  finite and study the SC2 in trivial and in the topological phase. Hereafter we set  $\tilde{\mu} = -0.01t$  so that  $V_Z^c \approx 0.027$  and use  $V_Z = 0.02t < V_Z^c$  for the trivial phase and  $V_Z = 0.05t > V_Z^c$  for the topological phase of the SC2. As long as  $V_Z$  is larger or smaller than  $V_Z^c$ , the results we will show are quite independent of



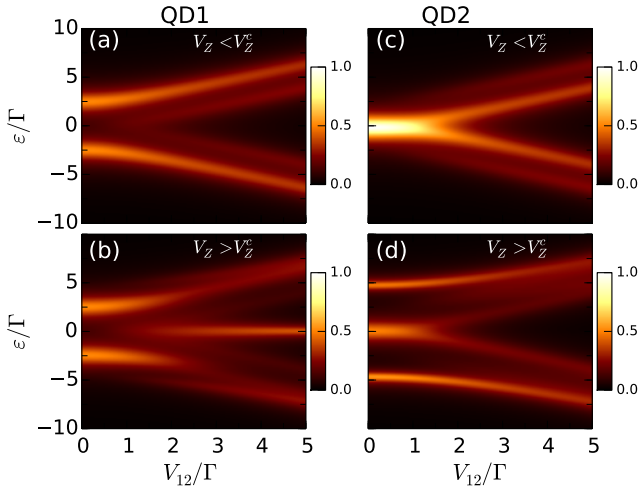


**Figure 4.** (Color online) Color map of the spin down local density of states (in unity of  $1/\pi\Gamma$ ) of the QD1 (left) and QD2 (right) as a function of the energy  $\varepsilon$  and the interdot coupling  $V_{12}$ . Top and lower panels show the results for the trivial and topological phase of the SC2, respectively.

$V_Z$ .

As we have seen above, the separation between the satellite peaks in the QD2 for the topological phase of the SC2 is much larger than the Andreev splitting, therefore, to make the results more visible, we now set the coupling between the dots and the superconductors  $V_1 = 0.008t$  and  $V_2 = 0.002t$  [39]. For these parameters and  $V_{12} = 0$  we have the following situation: the QD1 will always exhibit Andreev bound states because it is coupled to a normal superconductor. On the other hand, the QD2 will show a single particle peak if the SC2 is in its trivial phase ( $V_Z < V_Z^c$ ) and a zero mode corresponding to the Majorana mode leaked from the SC2 in addition to a two split peaks, for ( $V_Z > V_Z^c$ ). This three-peaks structure was extensively studied in our previous studies [32, 36].

In Fig. 4 we show a color map of the local density of states of the QDs as a function of the energy  $\varepsilon$  (vertical axis) and the inter-dot coupling  $V_{12}$  (horizontal axis). Let us start by analyzing these results in the normal phase of the superconductor SC2 ( $V_Z < V_Z^c$ , top panels).

In this regime,  $\rho_2^\downarrow$  [Fig. 4(c)] has just one peak at  $\varepsilon = 0$  while  $\rho_1^\downarrow$  [Fig. 4(a)] has two peaks located symmetrically about  $\varepsilon = 0$ . These two peaks correspond to the Andreev bound states discussed earlier. The single particle peak at  $\varepsilon = 0$  observed in  $\rho_2^\downarrow$  shows that the QD2 is not affected by the superconductors. The absence of Andreev states in the QD2 for  $V_{12} = 0$  is because the particle-hole asymmetry in the superconductor SC2 suppresses Andreev scatterings. As  $V_{12}$  increases, this scenario remains roughly unchanged in the atomic regime ( $V_{12} \lesssim \Gamma$ ) and is progressively changed as the system enters its molecular regime  $V_{12} \gtrsim \Gamma$ . In the molecular regime we note that  $\rho_1^\downarrow$  exhibits a four-peak structure very much similar to those of  $\rho_2^\downarrow$ . These peaks correspond to the Andreev bound states that are split by the interdot coupling. Note that while the inner peaks are weaker in  $\rho_1^\downarrow$  they are stronger in  $\rho_2^\downarrow$ , as compared to the outer ones. This is because the inner (outer) peaks of  $\rho_1^\downarrow$  ( $\rho_2^\downarrow$ ) corresponds to the ABS in QD2 (QD1) projected onto QD1 (QD2). The peaks appearing for positive and negative energies correspond to Andreev states on the “+” and “−” molecular orbitals, defined in Sec. 2.1. We will come back to this point and show the molecular density of states latter on in this section.

The results for the topological regime of the superconductor SC2 ( $V_Z > V_Z^c$ ) are shown in Figs. 4(b) and 4(d). We note in Fig. 4(b) that  $\rho_1^\downarrow$  is almost unchanged from the previous case in the atomic regime, with a two Andreev peaks in  $\rho_1^\downarrow$ . However, a complete different structure is seen in  $\rho_2^\downarrow$ . Note that even for  $V_{12} = 0$  we see the three-peaks structure known to be an indication of the leaking of the Majorana zero mode from the topological wire into the QD2 [32]. This scenario remains also roughly unchanged for the entire atomic regime ( $V_{12} < \Gamma$ ). Note that, because here the value of  $V_Z$  is smaller than in Fig. 2, here the satellite peaks are closer to each



other as compared to those of Fig. 2(d) for  $V_Z > V_Z^c$ . Moreover, the satellite peaks observed in  $\rho_2^\downarrow$  correspond to a Majorana state that is not bound to the QD2. Theoretically we can make it clear when we look at the Majorana spectral function as shown in Figs. 5 (shown only for  $V_Z > V_Z^c$ ). Observe that they appear only in  $\mathcal{D}_{B2}^\downarrow$  [Fig 5(d)] while the zero-energy peak is seen only for  $\mathcal{D}_{A2}^\downarrow$  [Fig 5(c)]. This shows that the nature of these peaks are completely distinct from the ABS. We should also emphasize that the zero-energy peak seen in Figs. 4(c) corresponds to a regular fermion state whereas the one in Fig. 4(d) corresponds to a Majorana bound state. Experimentally, the distinction between them can be made just by measuring the zero-bias conductance through the QD2 while changing the energy level of the QD2 in the regime of  $V_{12} \rightarrow 0$ . One would see that the conductance due to the Majorana peak would remain constant while in the regular fermion case it would show a peak. In fact, this corresponds to a remarkable signature of the Majorana bound state as one of us have discussed in Ref. [32].

The situation in the molecular regime ( $V_{12} > \Gamma$ ) is the opposite. In this regime, we see a three-peaks structure in  $\rho_1^\downarrow$  and two ones in  $\rho_2^\downarrow$ . Note that as  $V_{12}$  surpasses  $\Gamma$ , the Majorana zero energy peak dies off in the QD2 and arises in QD1 [compare the zero-energy peaks in the Figs. 4(b) and 4(d)]. This can be attributed to a second leaking of the Majorana from the QD2 into QD1. To support this interpretation, we now use the theoretical advantage of defining the Majorana GF. In Fig 5(a) and Fig 5(b) we show the spectral function of the Majorana operators  $\gamma_{A1}^\downarrow$  ( $\mathcal{D}_{A1}^\downarrow$ ) and  $\gamma_{B1}^\downarrow$  ( $\mathcal{D}_{B1}^\downarrow$ ), respectively, for the QD1 and in Figs 5(c) and 5(d), the same for the QD2. By comparing  $\mathcal{D}_{A2}^\downarrow$  with  $\mathcal{D}_{B2}^\downarrow$  from Fig 5(c) and Fig 5(d), respectively, we see that for  $V_{12} < \Gamma$  there is a zero-energy peak in  $\mathcal{D}_{A2}^\downarrow$  but none in  $\mathcal{D}_{B2}^\downarrow$ . On the other hand, there is no zero-energy peak in  $\mathcal{D}_{A2}^\downarrow$  nor in  $\mathcal{D}_{B2}^\downarrow$  for  $V_{12} > \Gamma$ . This indicates

that there is no single localized Majorana mode in the QD2. Now, if we look at QD1 Majorana spectral function [Figs. 5(a) and 5(c)] we see that there is no Majorana zero mode for  $V_{12} < \Gamma$ . However, as  $V_{12}$  becomes larger than  $\Gamma$ , while the Majorana  $\mathcal{D}_{A2}^\downarrow$  peak disappears from the QD2 it emerges at the QD1, as shown in  $\mathcal{D}_{A1}^\downarrow$ . This is the second leaking we have mentioned above.

The reader may ask what happens to the density of states for the spin *up*. To answer this question, in Fig 6 we show the spin *up* density of states in for the same set of parameters as in Fig. 4. Again, let us first look at the trivial phase of the SC2 ( $V_Z < V_Z^c$ ) shown in Figs. 6(a) and 6(c) for the QD1 and QD2, respectively. Comparing these plots with the corresponding ones in Fig. 4 we see that they are very much similar. This is because in the trivial phase, the SC2 is overall gaped and the Zeeman effect has no effect on the rest of the system, as we have already pointed out earlier. On the other hand, when we look at

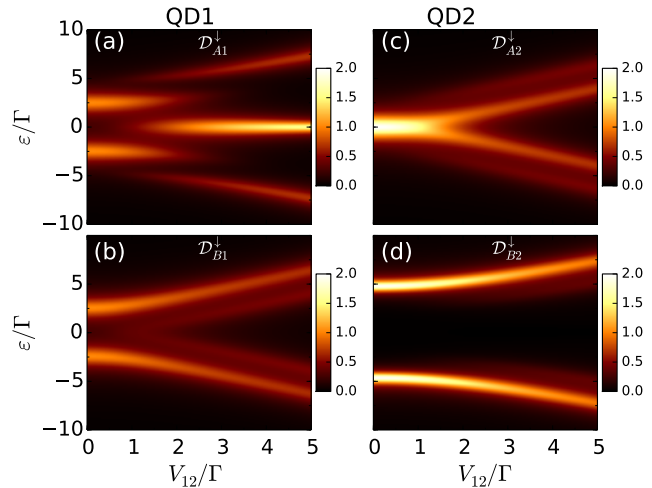


**Figure 5.** (Color online) Color map of the spin *down* Majorana spectral function (in unity of  $1/\pi\Gamma$ ) at the QD1 (left) and QD2 (right) vs the energy  $e$  and the interdot coupling  $V_{12}$ . Top and lower panels show the results for the topological phase of the wire 2, when we have a MBS. By comparing  $\mathcal{D}_A^\downarrow$  with  $\mathcal{D}_B^\downarrow$  for the same QD at the same energy, a peak appearing in only one of those shows there is a single Majorana mode. See discussion in the text.

the the topological phase of the SC2, shown in Figs. 6(b) and 6(d), and compare with Figs. 6(a) and 6(c), we see some small effect for finite energy even in the spin *up* electrons. This can be understood in the following way: because we have chosen  $V_z$  to be positive, the topological wire is strongly polarized with spin *down*. Therefore, the coupling between electrons with spin *up* in the dot and the Majorana in the SC2 is strongly suppressed. However, for finite  $V_{12}$  the QD2 is indirectly coupled to the normal superconductor SC2 via QD1 and an electron with spin *up* in the dot can couple to the Majorana mode via Andreev scatterings in the SC1. The effect is rather a small since this corresponds to very high order processes. This can also be seen in Fig.7, where we show the spin up Majorana spectral functions. Note that the spin up Majorana spectral functions for the QD2 shown in Fig 7(c) exhibit a signal of the zero mode coming from the spin down component.

To support our argument that in the molecular regime the Andreev states are bound to the molecule, while the Majorana mode is bound to

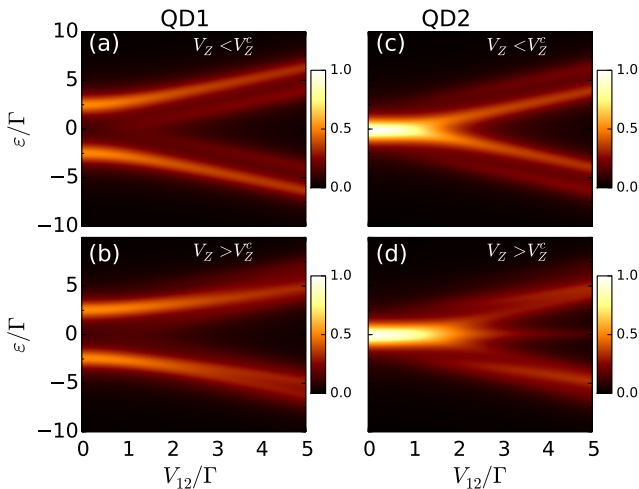


**Figure 6.** (Color online) Color map of the spin *up* local density of states (in unity of  $1/\pi\Gamma$ ) of the the QD1 (left) and QD2 (right) as a function of the energy  $\epsilon$  and the interdot coupling  $V_{12}$  for the same set of parameters as in Fig. 4.

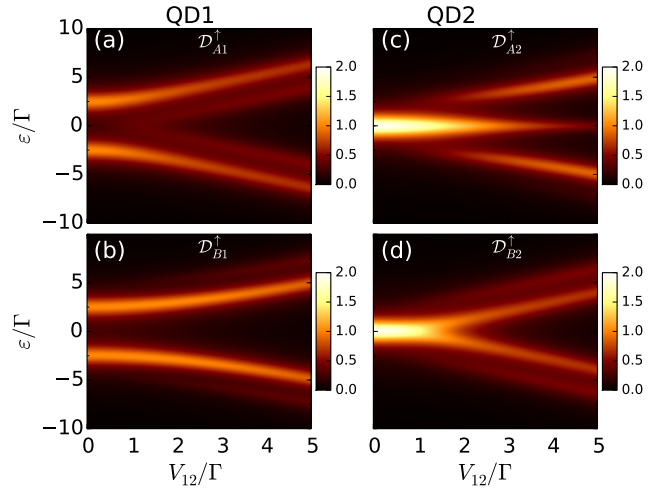


**Figure 7.** (Color online) Color map of the spin *up* Majorana spectral function (in unity of  $1/\pi\Gamma$ ) at the QD1 (left) and QD2 (right) vs the energy  $\epsilon$  and the interdot coupling  $V_{12}$ . Top and lower panels show the results for topological phase of the SC2. Note the  $\mathcal{D}_A^+$ ,  $\mathcal{D}_B^+$  in each dot are very similar showing that there is no spin *up* Majorana bound state in any of the QDs.

a particular QD (QD2, in our case), let us show the density of states for the molecular orbitals [defined in Eq. (15)]. In Fig. 8 we show the molecular density of states for spin *up* (top) and *down* (bottom) and both molecular orbitals (left and right). Note first that for  $V_{12} < \Gamma$  we see (for both orbital) three peaks for the spin *up* density of states and five peaks for the spin *down*. This is because in this regime, the molecular orbital corresponds, essentially, to the arithmetic mean value of the QD density of states shown previously. The central peak for spin *down*, corresponding to the Majorana state bound to the QD2, now appears on both molecular orbitals. The molecular density of states are more useful for  $V_{12} \gg \Gamma$ . In this regime, we note that for spin *up* [Fig. 8(a) and Fig. 8(c)] there are peaks only for negative energies in  $\rho_+^\uparrow$  whereas only positive energy peaks appear in  $\rho_-^\uparrow$ . Similarly,  $\rho_-^\downarrow$  and  $\rho_+^\downarrow$  [Figs. 8(b) and 8(d), respectively] exhibit a similar upper and lower branch of peaks but with a slightly more complex structures, because of the splitting of the

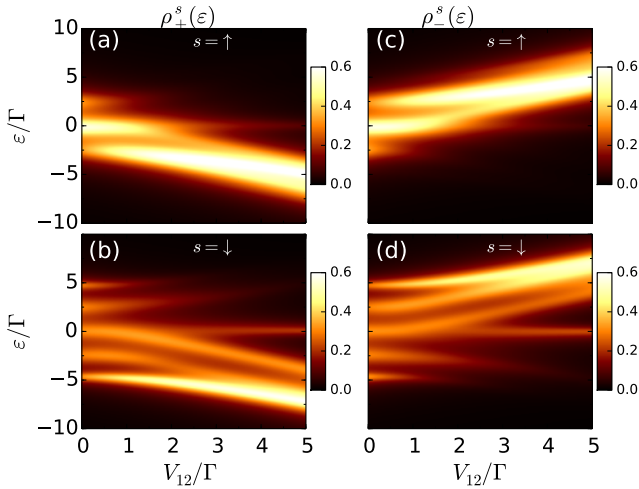


**Figure 8.** (Color online) Color map of the molecular density of states (in unity of  $1/\pi\Gamma$ ) vs energy and the interdot coupling. Left and right panels show the density of states for the symmetric and antisymmetric orbital, respectively while top and bottom show for the spin  $\uparrow$  and  $\downarrow$ , respectively. One can see the MBS in both maps characterized by the atomic regime.

central peak due to the interdot coupling, but the positive and negative energy peaks appear only in the “-” and “+” molecular orbitals, respectively. For  $V_{12} \ll \Gamma$  their position in energy increases almost linearly with  $V_{12}$ , which is characteristic of molecular orbitals. Interestingly, we note that there is a zero-energy peak that remains in both molecular orbitals. This indicates that this state is always bound to a QD. Indeed, as we have seen previously, this zero-energy peak corresponds to the Majorana mode bound to the QD2.

Similarly to what we have done in the single dot configuration, we now discuss how these features of the double-dot configuration could be observed within the current available experimental technology. This has to be done via local  $dI/dV$  measurement as in Ref. [6]. This is because in this configuration, the transport measurement between our lead 3 and 4 would not provide a local spectroscopy of the density of states of the QDs, individually. Therefore, similarly to the single-dot configuration, the STM

tip can be placed on top of an individual QD. The zero-energy feature of our plots could be obtained experimentally by fixing the gate voltage of the dots and controlling the interdot coupling, while measuring the  $dI/dV$  from the leads into the STM tip. Figure 9 shows the zero-energy LDOS vs interdot coupling for both trivial and topological phase of the SC2 for each QD, individually. The features seen in this figure were already present in the previous one but here, some of them are more apparent and deserves to be discussed. First, as we already noted earlier, we see that in the trivial regime ( $V_Z < V_Z^c$ ), even though the  $V_Z$  is finite the DOS is degenerate for spin *up* and *down*. This is because the application of a small Zeeman field in the SC2 does not affect the LDOS of the dots since there is no in-gap states of the SC2 that couples to the dot. This is not the case in the topological phase of the SC2 in which there is a MBS. Further, note the difference between the LDOS of the QD1 and QD2. Note that for  $V_{12} \ll \Gamma$ ,  $\rho_1^s(0) \ll \rho_2^s(0)$  (top panels). The suppression of the  $\rho_1^s(0)$  for  $V_{12} < \Gamma$  results from the presence of the Andreev bound states in the QD1. For

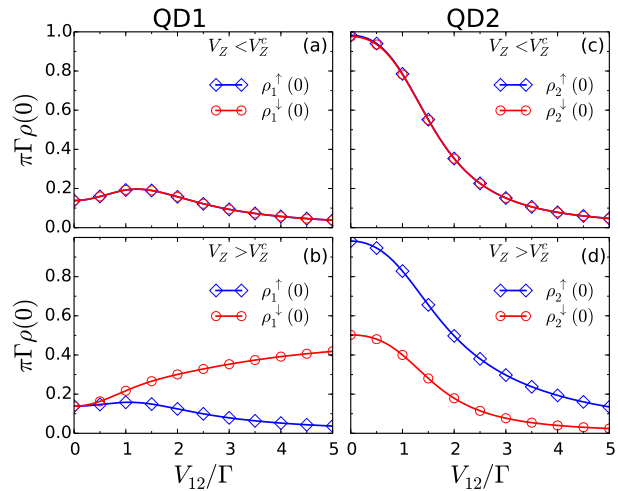


**Figure 9.** (Color online) Zero-energy LDOS of the QD1 (left) and QD2 (right) vs interdot coupling. Top and bottom panels show the results for the trivial and topological phase of the SC2, respectively. All the other parameters are the same as in Fig. 4.

$V_{12} \gg \Gamma$ , we see that both  $\rho_1^s(0)$  (both spins) decreases as the Andreev bound states take over the entire molecule. In the topological regime (bottom), the presence of the MBS leaked into the QD2 is manifested for  $V_{12} = 0$  as  $\pi\Gamma\rho_1^\downarrow(0) = 1/2$ , in agreement to what some of us have reported in Ref. [32]. As  $V_{12}$  increases, we see that  $\rho_2^\downarrow(0)$  decreases while  $\rho_1^\downarrow(0)$  increases, approaching  $1/2$ , because the MBS leaks into the QD1. Finally, as remarkable signature of the MBS, when we look only into the QD1 we note that while  $\rho_1^\uparrow(0)$  decreases and  $\rho_1^\downarrow(0)$  decreases for  $V_{12} \gg \Gamma$ , which produces strong polarization that could be detected using a spin polarized STM tip.

Another interesting point is that the signature of the topological quantum phase transition is still seen in the local density of states in the double dot configuration. To show this, in Fig. 10 we show the zero-energy density of states of the individual quantum dots vs  $V_z$  for the both, the atomic ( $V_{12} = \Gamma/2$ ) and the molecular regime ( $V_{12} = 5\Gamma$ ) in the top and lower panel, respectively. In the atomic regime (top panels) we see that a

jump in the  $\rho_2^\downarrow(0)$  at  $V_z = V_z^c$ . On the other hand, in the molecular regime (lower panels) the jump is overwhelmingly more pronounced in  $\rho_1^\downarrow(0)$  [Fig 10(b)] than the one observed in  $\rho_2^\downarrow(0)$  [Fig 10(d)]. For the spin *up* local density of states [diamonds (blue)], for both regimes and in both QDs we do not see any substantial change. The small jump in  $\rho_2^\uparrow(0)$  noticed in Fig. 10(d) [diamond (blue) line] results from a weak mixture of spin *up* and *down* in molecular regime due to Andreev scatterings. The results shown in Fig. 10 tell us that the topological quantum phase transition, well discussed in the single dot case, manifests itself even when the MBS and the ABSs coexist in the double double dot configuration. Moreover, alike in the single dot system, these features can be experimentally accessed in a simple spectroscopic tunneling measurement.

#### 4. Conclusion

Summarizing, we have studied the appearance of Andreev and Majorana bound states in a double quantum dot system. By studying the decoupled QDs configuration, we have shown that the MBS and the ABS cannot coexist in a single dot. This is because in the low-density regime (necessary for the topological phase of the superconductor) the electron-hole asymmetry suppresses the ABS. In the coupled dot configuration, one of the QDs (QD1) is coupled to a conventional superconductor that provides the Andreev bound states while the other (QD2) is coupled to a topological superconductor, providing the Majorana bound state in its topological phase. We show that in the trivial phase of the SC2, in the atomic limit of the system—where the interdot coupling is much smaller than the level broadening of the QDs ( $V_{12} \ll \Gamma$ )—the QD1 exhibits Andreev bound states while the QD2 exhibits a regular fermion state broadened by  $\Gamma$ . When the system is brought

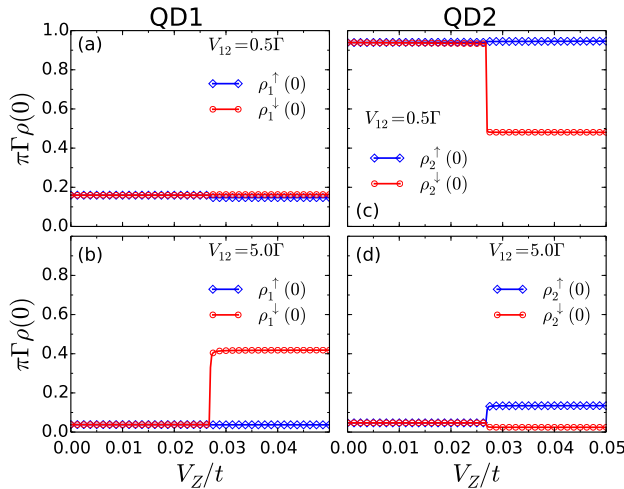


**Figure 10.** (Color online) Zero-energy LDOS of the QD1 (left) and QD2 (right) vs zeeman energy  $V_z$ . Top and bottom panels show the results for the atomic regime ( $V_{12} = \Gamma/2$ ) and molecular regime ( $V_{12} = 5\Gamma$ ), respectively. All the other parameters are the same as in Fig. 4.

into its molecular regime ( $V_{12} \gg \Gamma$ ), the Andreev bound states take over the entire molecule. More interestingly behavior occurs in the topological phase of the SC2. In this situation, we show that for  $V_{12} \ll \Gamma$  there are Andreev bound states in the QD1 for both spin components, while in the QD2 we find a Majorana bound state for spin *down* and Andreev bound states for spin *up*. In the molecular regime, on the other hand, the Majorana bound state leaks from the QD2 into the QD1, while the Andreev bound state can be seen in the entire molecule for the spin *up* component. These results reveal that, differently from the single dot case, the Majorana and the Andreev bound states coexist; while Andreev bound states can appear in molecular orbitals, the Majorana bound states is always bound to an atomic orbital. Another important feature that merits to be highlighted here is the remarkable signature of the topological quantum phase transition, manifested as a sharp jump in the zero-energy local density of states of the quantum dots, persisting even in the double dot case, in which the Majorana and the Andreev bound states coexist. Finally, we believe our results are relevant from both theoretical and experimental viewpoints and should stimulate future spectral tunneling measurements to detect the signatures of Majorana and Andreev bound states in the double dot system proposed here.

## Acknowledgments

We would like to thank the Brazilians agencies CAPES, CNPq (Grant N. 449488/2014-4) and FAPEMIG (Grant N. APQ-02344-14) for financial support. EV thanks C. Egues, L. G. G. V. Dias da Silva and D. Ruiz-Tijerina, for enriching comments and discussions.

## References

- [1] H. Suderow, E. Bascones, W. Belzig, F. Guinea and S. Vieira, Europhys. Lett. **50**, 749 (2000).
- [2] H. Suderow, E. Bascones, A. Izquierdo, F. Guinea, and S. Vieira, Phys. Rev. B **65**, 100519 (2002).
- [3] M. R. Buitelaar, T. Nussbaumer, and C. Schonenberger, Phys. Rev. Lett. **89**, 256801(2002).
- [4] J. A. Van Dam, Y. V. Nazarov, E. P. A. Bakkers, S. De Franceschi, and L. P. Kouwenhoven, Nature **442**, 667 (2006).
- [5] I. Weymann and P. Trocha, Phys. Rev. B **89**, 115305 (2014).
- [6] J-D. Pillet, P. Joyez, R. Žitko, and M. F. Goffman, Phys. Rev. B **88**, 045101 (2013).
- [7] S. De Franceschi, L. Kouwenhoven, C. Schonenberger, and W. Wernsdorfer, Nature Nanotech. **5**, 703 (2010).
- [8] R. Maurand, T. Meng, E. Bonet, S. Florens, L. Marty, and W. Wernsdorfer, Phys. Rev. X **2**, 019901 (2012).
- [9] K. J. Franke, G. Schulze, J. I. Pascual, Science **20**, 940 (2011).
- [10] D. Goldhaber-Gordon, H. Shtrikman, D. Mahalu, D. Abusch-Magder, U. Meirav, and M. A. Kastner, Nature **391**, 156 (1998).
- [11] A. V. Balatsky, I. Vekhter, and Jian-Xin Zhu Rev. Mod. Phys. **78**, 373 (2006).
- [12] J. Barański and T. Domański, Journal of Physics: Condensed Matter **25**, 435305 (2013).
- [13] T. Dirks, T. L. Hughes, S. Lal, B. Uchoa, Yung-Fu Chen, C. Chialvo, P. M. Goldbart, N. Mason, Nature Physics **7**, 386390 (2011).
- [14] Bum-Kyu Kim, Ye-Hwan Ahn, Ju-Jin Kim, Mahn-Soo Choi, Myung-Ho Bae, Kicheon Kang, Jong Soo Lim, Rosa Lpez, and Nam Kim, Phys. Rev. Lett. **110**, 076803 (2013)
- [15] A. Golub, I. Kuzmenko, and Y. Avishai, Phys. Rev. Lett. **107**, 176802 (2011).
- [16] D. E. Liu and H. U. Baranger, Phys. Rev. B **84**, 201308 (2011).
- [17] M. Lee, J. S. Lim, and R. Lopez, Phys. Rev. B **87**, 241402 (2013).
- [18] D. E. Liu, Meng Cheng, Roman M. Lutchyn, Phys. Rev. B **91**, 081405 (2015).
- [19] J. Alicea, Reports on Progress in Physics **75**, 076501 (2012).
- [20] A. Y. Kitaev, Phys.-Usp. **44**, 131 (2001).
- [21] N. Read and Dmitry Green, Phys. Rev. B **61**, 10267 (2000).
- [22] Jiannis K. Pachos, Steven H. Simon, New J. Phys.

**16** 065003 (2014).

- [23] Sankar Das Sarma, Michael Freedman, Chetan Nayak, Npj Quantum Inform. **1**, 15001 (2015).
- [24] A. R. Akhmerov, Phys.Rev. B **82**, 020509 (2010).
- [25] C. Laflamme, M. A. Baranov, P. Zoller, C. V. Kraus, Phys. Rev. A **89**, 022319 (2014).
- [26] Y. Oreg, G. Refael, and F. von Oppen, Phys. Rev. Lett. **105**, 177002 (2010).
- [27] C. Nayak, S. H. Simon, A. Stern, M. Freedman, and S. Das Sarma, Rev. Mod. Phys. **80**, 1083 (2008)
- [28] V. Mourik, K. Zuo, S. M. Frolov, S. R. Plissard, E. P. A. M. Bakkers, and L. P. Kouwenhoven, Science **336**, 1003 (2012).
- [29] M. T. Deng, C. L. Yu, G. Y. Huang, M. Larsson, P. Caroff, and H. Q. Xu, Nano Letters **12**, 6414 (2012).
- [30] A. Das, Y. Most, Y. Oreg, M. Heiblum, and H. Shtrikman, Nat. Phys. **8**, 887 (2012).
- [31] Roman M. Lutchyn, Jay D. Sau, and S. Das Sarma Phys. Rev. Lett. **105**, 077001 (2010).
- [32] E. Vernek, P. H. Penteado, A. C. Seridonio, J. C. Egues, Phys. Rev. B **89**, 165314 (2014).
- [33] D. Chevallier, P. Simon, and C. Bena, Phys. Rev. B **88**, 165401 (2013).
- [34] A. Golub, Phys. Rev. B **91**, 205105 (2015).
- [35] J. Alicea, Phys. Rev. B **81**, 125318 (2010).
- [36] D. A. Ruiz-Tijerina, E. Vernek, L. G. G. V. Dias da Silva, J. C. Egues, Phys. Rev. B **91**, 115435 (2015).
- [37] D. N. Zubarev, Sov. Phys. Usp. **3**, 320 (1960).
- [38] D. Rainis, L. Trifunovic, J. Klinovaja, and D. Loss, Phys. Rev. B **87**, 024515 (2013).
- [39] Different values of  $V_1$  and  $V_2$  would essentially modify the positions and the intensity of the Andreev peaks.